The Effect of Magnetic Balance and Particle Drifts on Radiating Divertor Behavior in DIII-D

T.W. Petrie 1), G.D. Porter 2), N.H. Brooks 1), M.E. Fenstermacher 2), J.R. Ferron 1),
M. Groth 2), A.W. Hyatt 1), R.J. La Haye 1), C.J. Lasnier 2), A.W. Leonard 1),
P.A. Politzer 1), M.E. Rensink 2), M.J. Schaffer 1), M.R. Wade 1), J.G. Watkins 3), and
W.P. West 1)

1) General Atomics, PO Box 85608, San Diego, California 92186-5608, USA
2) Lawrence Livermore National Laboratory, Livermore, California 94550, USA
3) Sandia National Laboratories, Albuquerque, New Mexico 87185, USA

e-mail contact of main author: petrie@fusion.gat.com

Abstract. Success of the *puff-and-pump* radiating divertor approach depends sensitively on both the divertor magnetic geometry and the ion $B \times \nabla B$ drift direction. In the puff-and-pump scenario used in this study, argon impurities were injected into the private flux region, while plasma flows into both the inner and outer divertors were enhanced by a combination of particle pumping near both divertor targets and deuterium gas puffing upstream of the divertor targets. For single-null (SN) configurations, argon accumulation was 2–3 times lower in the main plasma when the ion $B \times \nabla B$ drift was directed away from the divertor. The puff-and-pump approach was much less effective in screening argon from the main plasma of double-null (DN) discharges than of *SN* discharges, such that argon impurities accumulated in the main plasma of DNs at a rate ~2–3 times higher than in corresponding SNs. Regardless of which divertor in DN had argon injection, argon accumulated in the divertor that was *opposite* the $B \times \nabla B$ drift direction. The argon density in the main plasma during puff-and-pump operation fell by a factor of three for *dRsep* ≥ +0.4 cm when the ion $B \times \nabla B$ drift was directed away from the dominant divertor, and this represents the transition from DN to SN behavior during puff-and-pump application. Comparison of identically-prepared SN H-mode plasmas showed that core density control of deuterium and the argon was far more sensitive to the ion $B \times \nabla B$ drift direction than to divertor closure in DIII-D.

1. Introduction

Plasma heating of the divertor targets presents a major problem for the next generation of high power tokamaks. One way to ameliorate this problem is to inject impurities directly into the divertor, where these impurities, under certain conditions, can radiate a significant fraction of the plasma-conducted power before the plasma particles reach the divertor surface. Leakage of these impurities into the main plasma can be minimized by maintaining a strong flow of deuterium ions into the divertor through a combination of upstream deuterium gas puffing and active particle exhaust at the divertor targets, i.e., *puff-and-pump* [1–5]. This enhanced flow of deuterons toward the divertor targets exerts a frictional drag on impurities, inhibiting their escape from the divertor. The effectiveness of such puff-and-pump scenarios has been demonstrated on DIII-D [2,4,5]. A recent experiment [4] has demonstrated more than a two-fold reduction in the peak divertor heat flux in high performance H-mode single-null plasmas having moderate plasma beta (β_T = 2.8%), good confinement (H_{89p} = 2.0), and low core radiated power fraction ($P_{RAD,MAIN}/P_{IN} \approx 0.25$).

Both the direction of the toroidal magnetic field B_T and the degree of magnetic balance between divertors [i.e., the degree to which the plasma shape is considered single-null (SN) or double-null (DN)] have been shown previously to strongly impact both recycling [6] and particle pumping [7]. These observations raise questions whether the favorable results reported for SN in [4] extend to DN and whether these results depend on B_T direction. This is of interest because τ_E and β_T in tokamaks generally improve with highly-shaped DN cross-sections [8]. In this paper we evaluate plasma performance under puff-and-pump conditions, as the magnetic balance and/or the direction of B_T are changed.

2. Experimental Setup

We exploit the flexible shaping capabilities of DIII-D to make both balanced and unbalanced DN shapes with high-triangularity, and use the three cryopump rings to pump these shapes from both divertors simultaneously (Fig. 1). These cryopumps remove both deuterium and argon atoms. Argon was chosen for the injected impurity, because it radiates effectively at the temperatures prevailing in the divertor and pedestal regions of DIII-D H-mode plasmas and has a relatively short ionization mean-free path. Since the first wall and divertor armor are graphite, carbon is the dominant intrinsic impurity in DIII-D discharges.

To increase the deuteron flow toward these pumps, deuterium gas was introduced upstream of the divertor on the low-field side of the main plasma (Fig. 1). Argon could be injected into either private flux region (PFR). For the ELMing H-mode plasmas used in this study, typical plasma parameters were: $I_p = 1.2$ MA, $|B_T| = 1.75$ T, $q_{95} = 4.0$–4.4,

FIG. 1. Particle pumping and gas injection locations are shown together with the cross-section of a DN plasma.

$P_{IN} = (5$–$8)$ MW, $\bar{n}_e \approx (0.5$–$0.8) \times 10^{20}$ m^{-3} (or $\bar{n}_e/n_G = 0.4$–0.7), and $H_{89P} = 1.5$–2.0. We characterize the magnetic balance between divertors by radial separation between primary and secondary separatrices, given by $dRsep \equiv (R_L - R_U)$, where R_L is the radius at the outer midplane of the lower divertor separatrix flux surface and R_U is the radius at the outer midplane of the upper separatrix flux surface. For DN, $dRsep = 0$. In this study $dRsep$ ranges from -1.5 cm to $+1.5$ cm. We refer to configurations with $|dRsep| \geq 1$ cm as "SN", i.e., single null, even though the secondary null remains within the vacuum vessel.

Reversing the direction of B_T changes the vertical direction of the ion $B \times \nabla B$ particle drift, $V_{\nabla B}$; we will find it more physically meaningful to express our results in terms the ion-$B \times \nabla B$ drift direction, instead of B_T-direction. In particular, we refer to cases with the ion-$B \times \nabla B$ drift directed toward the top of the DIII-D vessel as "$V_{\nabla B\uparrow}$" and to those with the ion-$B \times \nabla B$ drift toward bottom of the vessel as "$V_{\nabla B\downarrow}$". This will be combined with the divertor geometry to describe the configuration, e.g., LSN-$V_{\nabla B\downarrow}$ or USN-$V_{\nabla B\downarrow}$ indicates the ion $B \times \nabla B$ drift is downward in a Lower or Upper single-null configuration respectively and DN-$V_{\nabla B\uparrow}$ indicates the ion $B \times \nabla B$ drift is upward in a DN configuration.

3. Results

3.1 Effect of changing the $B \times \nabla B$ direction on plasma fueling

In these experiments, changes in the pedestal density n_{PED} correlated far more strongly with the ion $B \times \nabla B$ drift direction than with modest differences in divertor geometry. As can be seen in Fig. 1, the upper divertor structure in DIII-D is more closed than the lower. Figure 2(a-d) shows four distinct SN arrangements: LSN-$V_{\nabla B\uparrow}$ (a), USN-$V_{\nabla B\downarrow}$ (b), LSN-$V_{\nabla B\downarrow}$ (c), and USN-$V_{\nabla B\uparrow}$ (d). In every case, the deuterium gas puff rate Γ_{D2} was 70 torr l/s. To match particle exhaust characteristics in the four cases, only the lower outer pump was activated for the cases in Fig. 2(a,c), and only the upper outer pump for the cases in Fig. 2(b,d). As shown in Fig. 2(e), the pedestal density for the two cases with $V_{\nabla B}$ *toward* the dominant divertor (LSN-$V_{\nabla B\downarrow}$ and USN-$V_{\nabla B\uparrow}$) was ≈30% greater than for the two *away from* the dominant divertor (LSN-$V_{\nabla B\uparrow}$ and USN-$V_{\nabla B\downarrow}$). Thus, the different closures of the upper and lower divertor had little effect on n_{PED}.
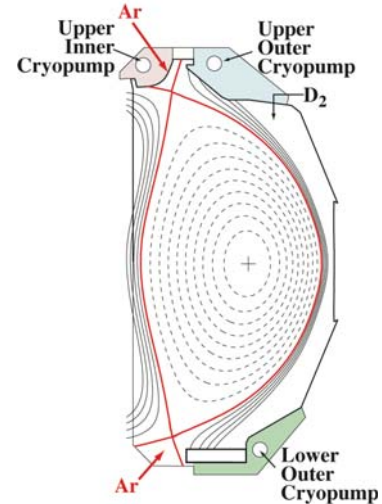
3.2 Effect of changing the ion $B \times \nabla B$ direction on argon behavior in SN plasmas

Both the accumulation of argon inside the main plasma and the removal of argon from the divertor were sensitive to the $V_{\nabla B}$ direction. Figure 3 compares case USN-$V_{\nabla B\downarrow}$ with case USN-$V_{\nabla B\uparrow}$ [Fig. 2(b,d)]. Argon was injected into the PFR of the upper divertor and all three cryopumps were operational. Both cases had $\Gamma_{D2} = 108$ torr l/s and a steady argon puff rate $\Gamma_{Ar} = 1$ torr l/s, [Fig. 3(a)]. As in the above, n_{PED} was greater for the USN-$V_{\nabla B\uparrow}$ case than for the USN-$V_{\nabla B\downarrow}$ case [Fig. 3(b)]. The inner leg of the divertor in the USN-$V_{\nabla B\uparrow}$ case partially detached near $t = 3.6$ s, when the divertor radiated power $P_{R,DIV}$ showed a rapid increase typical for these operating conditions in DIII-D [Fig. 3(c)]. Argon accumulation in the core was ≈3.5 times higher for USN-$V_{\nabla B\uparrow}$, as evidenced by the density of the dominant Ar^{16+} charge state $n_{Ar^{+16}}$ at ρ=0.7 [Fig. 3(d)]; for similar discharges, detailed analysis with the MIST [9] impurity transport code indicates that $n_{Ar^{+16}}$ should be >80% of n_{Ar} at ρ ≈ 0.7. The carbon concentration in the core was little changed by argon injection, as evidenced by the density of the dominant C^{6+} charge state at ρ=0.7 [Fig. 3(e)]. The rate at which argon was exhausted by the *upper outer* divertor cryopump Γ_{P-Ar} was much higher for the USN-$V_{\nabla B\downarrow}$ case [Fig. 3(f)]: ≈85% of the injected argon was removed by the pump in the outer divertor for USN-$V_{\nabla B\downarrow}$ compared with ≈35% for the USN-$V_{\nabla B\uparrow}$.

3.3 Effect of changing the ion $B \times \nabla B$ direction on argon behavior in DN plasmas

Regardless of whether argon is injected into the upper or lower divertor of DN plasmas, we find that measurable increases in radiated power occurs in the divertor *opposite* the direction of $V_{\nabla B}$, and argon pumping is also stronger there; little radiative response and argon pumping is observed in the divertor into which $V_{\nabla B}$ points. Argon was injected into the upper divertor (Fig. 4) and into the lower divertor (Fig. 5). In Fig. 4(b,c) a measureable response to argon injection was observed in the lower divertor for (DN-$V_{\nabla B\uparrow}$, solid) and in the upper divertor for (DN-$V_{\nabla B\downarrow}$, dashed). More than two-thirds of the injected argon was pumped from the
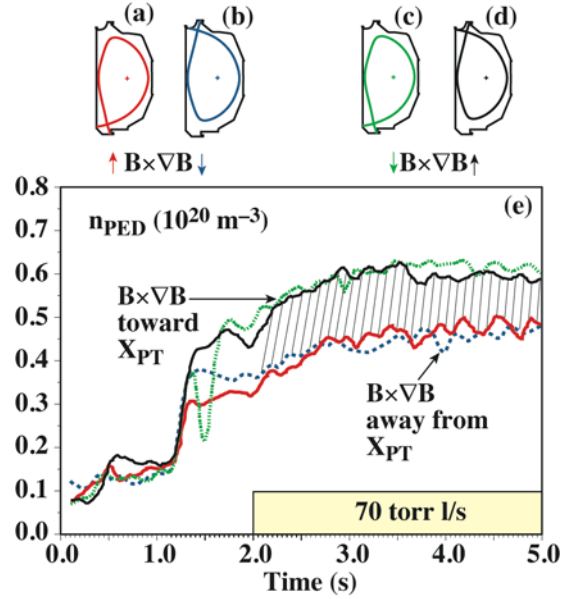

FIG. 2. (a-d) The four plasma shapes discussed in Sec. 3.1 are shown, together with the direction of $V_{\nabla B}$. (e) n_{PED} for these four cases is shown.
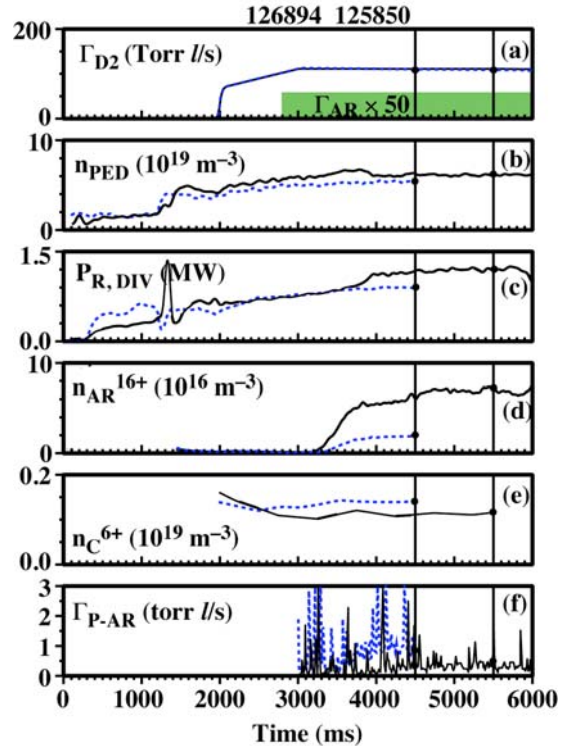

FIG. 3. The waveforms of (a) the Γ_{D2} and Γ_{Ar} gas puffs, (b) n_{PED}, (c) $P_{R\text{-}DIV}$, (d) $n_{Ar^{+16}}$, (e) $n_{C^{6+}}$, and (f) $\Gamma_{P\text{-}Ar}$ are shown for $V_{\nabla B}$ *toward* the divertor (solid) and *away from* the divertor (dashed).

upper divertor for the DN-$V_{\nabla B\downarrow}$ case, but less than one-third of argon was pumped in the $V_{\nabla B\uparrow}$ case [Fig. 4(d)]. When argon was injected into the PFR of the lower divertor, a radiative response was observed only in the divertor opposite the $V_{\nabla B}$ direction, and again a much higher fraction of argon was exhausted by the upper outer pump for the DN-$V_{\nabla B\downarrow}$ case [Fig. 5(d)]. The dependence of the divertor radiated power buildup on $V_{\nabla B}$ direction is consistent with the up/down asymmetry observed in argon accumulation between the two divertors [5].
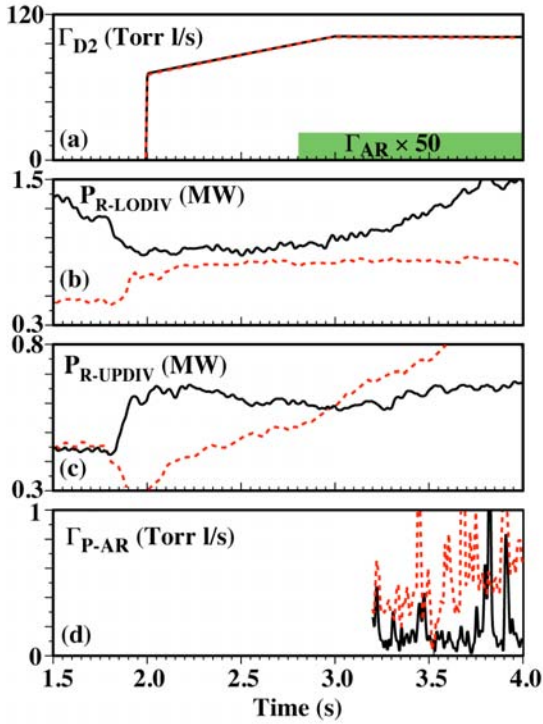

FIG. 4. Cases where argon is injected into the upper divertor PFR of DN plasmas: The waveforms of (a) the Γ_{D2} and Γ_{Ar} gas puff programs, (b) $P_{R\text{-LODIV}}$, (c) $P_{R\text{-UPDIV}}$, and (d) $\Gamma_{P\text{-Ar}}$ are shown vs time: $V_{\nabla B\uparrow}$ (solid) and $V_{\nabla B\downarrow}$ (dashed).
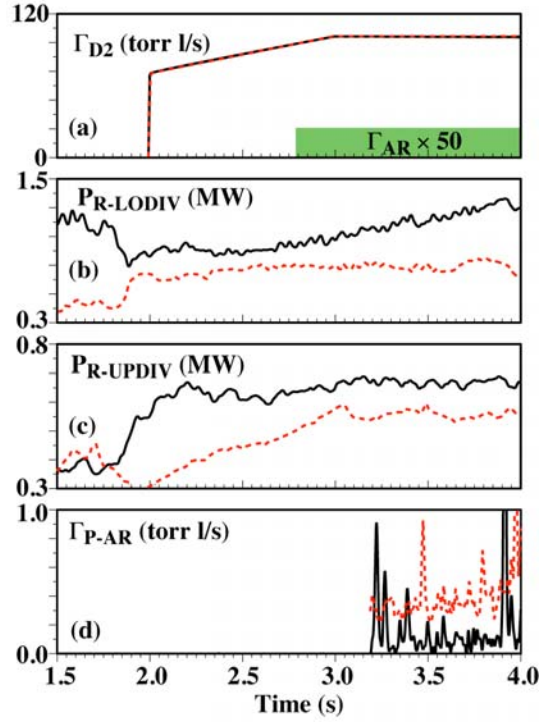
FIG. 5. Cases where the argon is injected into the lower divertor PFR of DN plasmas. Same waveforms as in Fig. 4

3.4 Comparison of SN with DN plasmas during puff-and-pump operation

Figure 6 shows the *initial* rate $d/dt(n_{Ar})$ at which the argon accumulated in the main plasma of SNs and DNs as a function of Γ_{Ar} (with fixed Γ_{D2}). Argon was injected into the PFR of the *upper* divertor. Given the same Γ_{Ar}, n_{Ar} increased in DN-$V_{\nabla B\downarrow}$ at roughly twice the rate that it did in the USN-$V_{\nabla B\downarrow}$ case. Reversing the direction of $B \times \nabla B$ did not appreciably change the ratio of $d/dt(n_{Ar})$ between the DN-$V_{\nabla B\uparrow}$ and USN-$V_{\nabla B\uparrow}$ cases. In the DN-$V_{\nabla B\uparrow}$ cases, however, $d/dt(n_{Ar})$ was considerably higher than that in the DN-$V_{\nabla B\downarrow}$ cases. Figure 6 shows that the lower the fraction of argon exhausted by the upper outer divertor pump, the higher the rate of buildup of argon in the main plasma.

We next evaluate argon buildup in the main plasma by varying Γ_{D2} while fixing Γ_{Ar}. Argon was injected into the PFR of the upper divertor of these DN and upper SN plasmas. Both ion $B \times \nabla B$ drift directions are considered. In all four cases, n_{Ar} initially decreased with increasing $\Gamma_{D2} \leq 70$ torr l/s (Fig. 7). While n_{Ar} decreased monotonically with increasing Γ_{D2} for the USN-$V_{\nabla B\downarrow}$, the highest level of Γ_{D2} produced in an increase in the core argon

concentration in the other three cases, particularly in both DN cases. The n_{Ar} values were comparable for DN-$V_{\nabla B\downarrow}$ and USN-$V_{\nabla B\downarrow}$ when $\Gamma_{D2} \leq 70$ torr l/s, but diverged sharply when Γ_{D2} was raised to 100 torr l/s. At the highest Γ_{D2}, the inner divertor leg of the DN-$V_{\nabla B\downarrow}$ case was only tenuously attached (e.g., electron density $n_{IN\text{-}DIV}$ and temperature $T_{IN\text{-}DIV}$ were $\leq 1 \times 10^{19}$ m^{-3} and ≤ 10 eV, respectively) during the puff-and-puff phase. For USN-$V_{\nabla B\downarrow}$, on the other hand, $n_{IN\text{-}DIV}$ and $T_{IN\text{-}DIV}$ were $\approx 10^{20}$ m^{-3} and 10–20 eV, respectively. The escape of neutral argon through the upper inner leg to the high-field side SOL is far more likely in the DN-$V_{\nabla B\downarrow}$ case, since the mean-free path of neutral argon through the upper inner divertor region is at least an order of magnitude larger than for the above USN-$V_{\nabla B\downarrow}$ case.

3.5 Argon accumulation into the core plasma near balanced DN as *dRsep* is varied

Argon accumulation in the main plasma was reduced significantly for *dRsep* values of >0.4 cm for $V_{\nabla B\downarrow}$ cases (Fig. 8). A factor of 3 decrease in n_{Ar} was observed between *dRsep* = 0 and *dRsep* = +0.4 cm, with only a slight decrease when *dRsep* was raised further [Fig. 8(a)]. The local maximum in n_{Ar} and n_{PED} near +0.25 cm is likely associated with an improvement in H_{89p} [Fig. 8(b,c)]. Since $H_{89p} \approx 1.5$ for both *dRsep* = 0 and *dRsep* = +0.4 cm cases, the change in n_{Ar} was not due to a change in confinement time. Note that for *dRsep* ≥ 0.5 cm, $D_{\alpha\text{-}IN}$ is little changed, indicating that the attachment at the inner divertor target characteristic of USN-$V_{\nabla B\downarrow}$ plasmas is fully established [Fig.8(d)]. For shots similar to those discussed in this section, the scrape-off width (λ_p) of the parallel heat flux density at the outboard midplane was ≈ 0.4 cm for *dRsep* = +0.4 cm [Fig. 8(e)] [10].

FIG. 6. The initial rates of argon accumulation in USN and DN plasmas $d/dt(n_{AR})$ are plotted vs Γ_{Ar} for both $V_{\nabla B\downarrow}$ and $V_{\nabla B\uparrow}$ cases. The percentage of argon pumped by the upper outer cryopump is noted.

FIG. 7. n_{Ar} is plotted vs Γ_{D2} under four distinct conditions.

4. Discussion

Pedestal density exhibits much more dependence on the direction of $V_{\nabla B}$ than on the relative closure of the divertors. The importance of particle drifts in fueling has been suggested in Ref. [11], where the most significant fueling of the main plasma was shown to occur on the high field side near the X-point. As such, the differences between upper and lower divertors in DIII-D would have a secondary role in fueling.

Different plasma behavior was observed during puff-and-pump operation for the USN-$V_{\nabla B\downarrow}$ and USN-$V_{\nabla B\uparrow}$ cases discussed in Sec. 3.2. UEDGE [12] edge transport analysis,
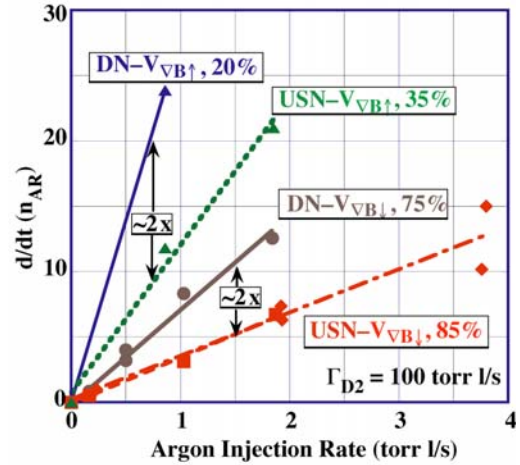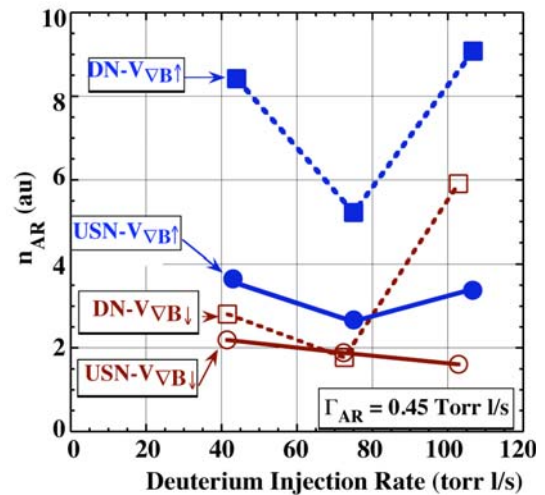
which includes a full particle drift package applied to H-mode SN plasmas with finite *dRsep*, highlights the importance of these drifts to seed impurity behavior.

The net deuterium flows in the USN-$V_{\nabla B\uparrow}$ case, as calculated by UEDGE, are shown in Fig. 9(a), and for the USN-$V_{\nabla B\downarrow}$ case in Fig. 9(b). The $E_r \times B$ drift (red arrows in Fig. 9(a,b) is largely responsible for plasma flow across the PFR toward the inner strike point for USN-$V_{\nabla B\uparrow}$ [Fig. 9(a)] and in the opposite direction for USN-$V_{\nabla B\downarrow}$ [Fig. 9(b)]. The radial electric field E_r is determined largely by the electron temperature gradient normal to the local flux surfaces. These poloidal particle flows across the PFR were previously measured in DIII-D divertor plasmas and found to be consistent with the particle flow predicted by modeling [13]. Because of this $E_r \times B$ flow, UEDGE predicts that much of the injected argon ionized in the PFR is preferentially swept toward the *inner* divertor target for $V_{\nabla B\uparrow}$, and preferentially toward the outer divertor target for USN-$V_{\nabla B\downarrow}$. The resulting UEDGE distribution of argon at trace level

FIG. 8. (a) n_{Ar}, (b) n_{PED}, (c) H_{89P}, and (d) I_p are shown vs *dRsep*. Argon was injected into the upper divertor PFR. The solid vertical line is the approximate transition from *DN*-to-*SN* behavior during puff-and-pump.

is shown in Fig. 9(c) for USN-$V_{\nabla B\uparrow}$ and for USN-$V_{\nabla B\downarrow}$ in Fig. 9(d). In the former case, the increase in argon at the inner target would enhance the local radiated power near the inner target, and at large enough levels lead to a detached *inner* divertor leg, as observed in Fig. 3. For USN-$V_{\nabla B\downarrow}$, the injected argon would be preferentially swept toward the *outer* divertor target. Although electron temperature and the peak heat flux would be reduced at the outer divertor target, detachment of the outboard leg from the divertor target did not occur at the Γ_{Ar} and Γ_{D2} used in this experiment. Sweeping of argon toward the outer target in the USN-$V_{\nabla B\downarrow}$ case is reflected by the UEDGE prediction that the argon exhaust rate by the outer divertor cryopump is two-and-half times higher for USN-$V_{\nabla B\downarrow}$ than USN-$V_{\nabla B\uparrow}$, which is consistent with experiment. Less pumping of argon from the upper outer divertor target implies that unpumped argon will eventually leak out of the divertor at a higher rate for USN-$V_{\nabla B\uparrow}$ than for USN-$V_{\nabla B\downarrow}$ and serve as a source of argon "fueling" for the main plasma. UEDGE analysis indicates that a strong particle drift toward the lower divertor on the high field side SOL, largely driven by the $E_r \times B$ drift, facilitates the escape of argon from the upper divertor for USN-$V_{\nabla B\uparrow}$ [Fig. 9(a)]. The ratio of argon accumulation in the main plasma for USN-$V_{\nabla B\uparrow}$ to that for USN-$V_{\nabla B\downarrow}$, ($n_{Ar-\nabla B\uparrow}/n_{Ar-\nabla B\downarrow}$), is $\approx 3.5/1$ for experiment and $\approx 20/1$ for UEDGE analysis. Details of the modeling will be discussed in a future paper.

For DN plasmas, argon that was injected into the PFR of the divertor toward which $V_{\nabla B}$ was directed accumulated faster in the main plasma. When argon was injected into the PFR of the upper divertor, the fraction of argon pumped by the upper outer divertor was again higher for the DN-$V_{\nabla B\downarrow}$ case ($\approx 75\%$) than for the DN-$V_{\nabla B\uparrow}$ case ($\approx 20\%$). Because the same particle drifts are in play for both DNs and SNs, it is not surprising that this result for DNs is similar to that found above in the SNs. Hence, the leakage of argon particles from the upper
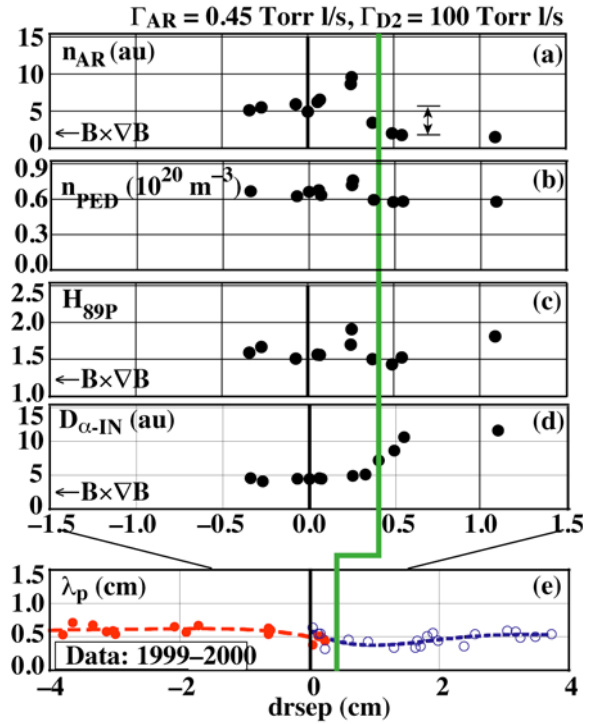
outer divertor is greater for DN-$V_{VB\uparrow}$ than for a corresponding DN-$V_{VB\downarrow}$ case, and, as with the SN, more of the injected argon would then be available to "fuel" the main plasma in $V_{VB\uparrow}$. Strong up/down asymmetries in the divertor radiated power and the poloidal distribution of argon were observed. Though argon was injected from a single poloidal location in the PFR of the upper divertor, argon accumulated in the divertor opposite the V_{VB} direction, leading to a greater increase in the radiated power from that divertor compared with the other.

Argon buildup in the core plasma of DNs was higher than in comparable SNs with the same V_{VB} direction. While the same particle drifts are in play for both DNs and SNs, DNs differ in two important ways from SNs. Power flows out of the core plasma primarily on the low field side [10] and roughly half of this power is in principle available for maintaining plasma attachment at the inboard target of a SN [14]. In a DN, power flowing into the SOL on the low-field side is instead shunted to the two outer divertor targets, starving the inner divertor targets of the power needed to maintain plasma ionization. Thus, the characteristic electron temperature for the inboard SOL plasma of a DN is less than that of a comparable SN, while the SOL density profile is also narrower for the DN [6]. Since both inner divertor targets are only tenuously attached (and sometimes detached) in DNs, it is relatively direct for argon neutrals to leak out of the upper divertor and into the SOL on the high-field side, and once there, to have easier access the main plasma than SN. In addition, the SOL on the high field side of the DN is largely quiescent, because the ELMs, initiating on the low-field side,

FIG. 9. The deuterium particle flows in upper *SN* plasmas, as calculated by UEDGE. (a) $V_{VB\uparrow}$ case and (b) $V_{VB\downarrow}$ case. Resulting argon distribution for (c) $V_{VB\uparrow}$ case and (d) $V_{VB\downarrow}$ case.

are isolated from the high field SOL plasma [15]. ELMing activity expels impurities, which have just penetrated the separatrix of the core plasma, thus making it less likely for argon impurities to accumulate in the core. The lack of ELMing on the high field side of double-null plasmas facilitates argon "fueling" from the high field side. Thus, effective radiative divertor operation with DN plasmas would benefit significantly if the inner divertor leg(s) maintain attachment to inhibit leakage of the radiating impurity into the core.

The leakage of argon out of the divertor and its subsequent buildup inside a SN plasma was reduced by raising Γ_{D2} when the V_{VB} direction was out of the divertor. However,
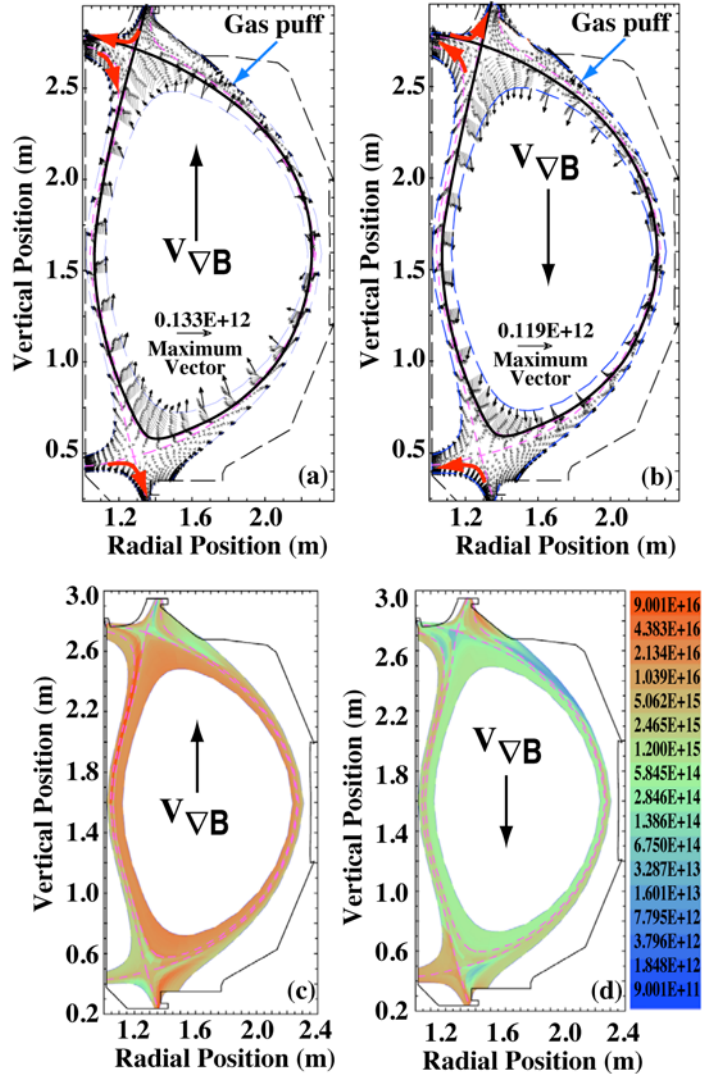
increasing Γ_{D2} was much less effective in this regard when the $V_{\nabla B}$ direction was into the divertor. For DNs, this solution was least effective. Gas puffing from the low-field side of the DN enhances the deuterium flow into the two divertors on the low-field side, but was ineffective in enhancing deuterium flow into the high-field side divertors, as the high-field SOL is severed magnetically from the low-field SOL. Because the particle removal rates of argon by both outer divertor pumps depend strongly on the direction of $V_{\nabla B}$, Γ_{D2} that might be effective in trapping impurities for one divertor might not be as effective in trapping impurities in the other. The poloidal redistribution of the argon impurities suggests that particle drifts are important and their role is presently under investigation with UEDGE. Our results clearly highlight the difficulty in equalizing radiated power between divertors.

As the magnetic balance shifts from DN to SN, an increasing fraction of the power flow from the low-field SOL transits to the inner target. In Sec. 3.5, we found significantly reduced argon in the core plasma when *dRsep* was raised above +0.4 cm for $V_{\nabla B \downarrow}$; this value of *dRsep* is comparable to the width of the heat flux profile λ_p. With *dRsep* ≥ +0.4 cm, significant power flow from the low-field side SOL can reach the high field side target and maintain sufficient density and temperature to impede the escape of neutral argon to the high field side SOL. Increasing *dRsep* further only leads to marginally more power reaching the inner target and minimal change in recycling activity, as evidenced by the behavior of $D_{\alpha\text{-IN}}$ in Fig. 8d. In terms of the plasma that the argon "sees" at the inner target, discharges with *dRsep* ≥ +0.4 cm much more closely resemble the USN plasmas than DN plasmas.

5. Conclusion

We have shown that the contributions from both particle drifts and magnetic balance can strongly impact performance of diverted tokamaks under puff-and-pump conditions. We find that the nearest to DN that puff-and-pump can be applied but still maintain low impurity contamination of the main plasma was *dRsep* ≈ 0.4 cm with the ion $B \times \nabla B$ drift directed away from the dominant divertor. Even for tokamaks characterized as strongly SN, such as ITER, the results presented here point to the importance of considering particle drifts in assessing the effects of a puff-and-pump radiating divertor approach.

Acknowledgment

References

[1]   SCHAFFER, M.J., *et al.*, J. Nucl. Mater. **241-243**, 585 (1997).
[2]   WADE, M.R., *et al.*, Nucl. Fusion **38**, 1839 (1998).
[3]   GOETZ, J.A., *et al.*, J. Nucl. Mater. **266-269**, 359 (1999).
[4]   PETRIE, T.W., *et al.*, J. Nucl. Mater. **363-365**, 416 (2007).
[5]   PETRIE, T.W., *et al.*, Nucl. Fusion **48**, 045010 (2008).
[6]   PETRIE, T.W.., *et al.*, J. Nucl. Mater. **313-316**, 834 (2003).
[7]   PETRIE, T.W., *et al.*, Nucl. Fusion **46**, 57 (2006).
[8]   LAO, L.L., *et al.*, Nucl. Fusion **41**, 295 (2001).
[9]   HULSE, R.A., Nucl. Technol. Fusion **3**, 259 (1989).
[10]   PETRIE, T.W., *et al.*, J. Nucl. Mater. **290-293**, 935 (2001).
[11]   GROTH, M., *et al.*, J. Nucl. Mater. **337-339**, 452 (2005).
[12]   ROGNLIEN, T.D., *et al.*, Phys. Plasmas **34**, 362 (1994).
[13]   BOEDO, J.A., *et al.*, Phys. Plasmas **7**, 1075 (2000).
[14]   LEONARD, A.W., *et al.*, J. Nucl. Mater. **220-222**, 325 (1995).
[15]   PETRIE, T.W., *et al.*, Nucl. Fusion **43**, 910 (2003).